# JOURNAL OF THEORETICAL AND APPLIED MECHANICS

**63**, 4, pp. 795–807, Warsaw 2025 https://doi.org/10.15632/jtam-pl/209747

# EFFECT OF FATIGUE ON THE MICROHARDNESS OF SCRAP CROSS-SECTIONS AFTER CYCLIC BENDING WITH TORSION OF RG7 BRONZE ALLOY

Mariusz PRAŻMOWSKI\*, Joanna MAŁECKA, Tadeusz ŁAGODA

Mechanical Engineering, Opole University of Technology, Opole, Poland \*corresponding author, m.prazmowski@po.edu.pl

This work analyzes the effect of fatigue on the microhardness of the fracture plane of bronze samples. The analysis will be based on tests under conditions of cyclic bending, cyclic torsion, and two combinations of bending and torsion of samples made of RG7 bronze. All tests were performed at zero mean stress. The fracture plane was divided into a grid at 0.4 mm intervals, and local microhardness values were determined. On this basis, contour lines of microhardness were determined. The analysis of these contours on the surface showed that the most significant increase in the maximum microhardness in relation to the starting material was obtained for the static tension and cyclic bending tests. However, for the combination of cyclic bending and torsion, a minimal influence of shear stress in the maximum microhardness was obtained.

Keywords: fatigue life-time; bending with torsion; micro hardness; fracture plane.



Articles in JTAM are published under Creative Commons Attribution 4.0 International. Unported License https://creativecommons.org/licenses/by/4.0/deed.en. By submitting an article for publication, the authors consent to the grant of the said license.

#### 1. Introduction

The relationship between strength and hardness of a material is well known. This also applies to the influence of material hardness on fatigue life. This influence can be found in numerous publications. Some papers also propose full formulas in which the fatigue strength (fatigue strength limit) is a function of hardness, or even, on this basis, full fatigue characteristics can be determined. The test results of the Ni alloy samples showed that as the size of the crystallites decreased, the experimental fatigue life of the samples increased (Sriraman et al., 2007). This is due to the increase in the Vickers hardness (HV) value. In (Bandara et al., 2016), the S-N fatigue characteristics in the range from small to gigacycles for steel with a tensile strength not exceeding 1400 MPa were derived and verified. This characteristic is an empirical characteristic based on the Brinell hardness (HB) of the analyzed steel and has the typical form for this range, i.e., the letter S as presented, among others, in (Kurek et al., 2019). It was verified on the basis of fatigue tests with different cycle asymmetry coefficients for samples with and without a notch. In (Assi & Alkalali, 2021), the analysis of 5 steels and 5 aluminum alloys revealed that the fatigue limit in these two material groups depends linearly on HB.

Görzen *et al.* (2022) found that there is a linear relationship between the fatigue limit and HV, based on fatigue tests of five steels: X0.5CuNi2-2, X21CuNi2-2, 42CrMo4, 100CrMnSi6-4, and C50E.



This publication has been funded by the Polish Ministry of Science and Higher Education under the Excellent Science II programme "Support for scientific conferences".

The content of this article was presented during the 61st Symposium "Modelowanie w mechanice" (Modelling in Mechanics), Szczyrk, Poland, March 2–5, 2025.

Roessle & Fatemi (2000) proposed the deformation characteristics as a function of HB. This relationship is a quadratic function due to the hardness in the following form:

$$\frac{\Delta\varepsilon}{2} = \frac{4.25 \,\mathrm{HB} + 225}{E} \,(2N_f)^{-0.09} + \frac{0.32 \,\mathrm{HB}^2 - 487 \,\mathrm{HB} + 191000}{E} \,(2N_f)^{-0.56} \,. \tag{1.1}$$

In (Shamsaei & Fatemi, 2009), for 1050 steel in three different states, which resulted in 3 different hardnesses (198, 360, and 565 HB) and different fatigue characteristics, an analogous expression to Eq. (1.1) was proposed, except that it is dependent on shear deformation on HB by modifications of the Fatemi–Socie model for multiaxial load condition:

$$\frac{\Delta \gamma_{\text{max}}}{2} \left( 1 + k \frac{\sigma_{n,\text{max}}}{\sigma_y} \right) = \frac{6.37 \,\text{HB} + 338}{E} \left( 2N_f \right)^{-0.09} + \frac{0.55 \,\text{HB}^2 - 842 \,\text{HB} + 331000}{E} \left( 2N_f \right)^{-0.56}, \tag{1.2}$$

where

$$k = (0.0003 \,\text{HB} + 0.0585) \,(2N_f)^{0.09}$$
 (1.3)

Other methods have also been proposed, including those based on the ultimate tensile strength, i.e.,  $\sigma_B$ :

- Mitchell model (Mitchell, 1996):

$$\sigma_B = 3.45 \,\mathrm{HB},\tag{1.4}$$

- Roessle-Fatemi model (Roessle & Fatemi, 2000):

$$\sigma_B = 0.0012 \,\text{HB}^2 + 3.3 \,\text{HB},\tag{1.5}$$

- Baumel-Seeger recommendation and Kloos-Velten model (Kloos & Velten, 1984):

$$\sigma_B = 3.29 \,\text{HV} - 47 \quad \text{for} \quad \text{HV} \le 445,$$
(1.6)

$$\sigma_B = 4.02 \,\text{HV} - 374 \quad \text{for} \quad \text{HV} < 445,$$
(1.7)

- method proposed in (Shiozawa & Sakai, 1996):

$$\sigma_B = \frac{\text{HV} - 1.837}{0.304}.\tag{1.8}$$

Li et al. (2015) summarized the relationships between fatigue strength and ultimate stress as well as hardnesses expressed by HV, HB, and HRC (Rockwell hardness). The list of 14 linear or square relationships between fatigue limit and the same hardness was made on the basis of proposals from the literature on testing such materials as: steels and aluminum, copper, titanium, and magnesium alloys for the first relationship, and steel (Pang et al., 2014) and Cu-Be alloy (Pang et al., 2013) for hardness. The proposed dependencies in the hardness function are simple, linear or square mathematical functions of the hardness of the analyzed materials.

James *et al.* (2009) found that hot spot strain in a welded joint is a linear function of HV versus residual strain. This, in turn, has a linear (double-logarithmic) effect on the experimental life time.

Xin et al. (2021) proposed the four-parameter Bandara stress fatigue characteristic for welded joints (Bandara et al., 2015; 2016):

$$\sigma_a = a(N_f + B)^b + c, (1.9)$$

where the coefficients a, B, and c were determined based on various physical quantities, including the HV of the tested material. The exponent b was assumed as constant, equal to -0.20.

Kondo *et al.* (2003), based on measurements and analyses, showed that the stress intensity factor is linearly dependent on the HV according to the following equation:

$$\Delta K_{th} = 3.3 \cdot 10^{-3} (\text{HV} + 120) \left(\sqrt{\text{area}}\right)^{1/3}.$$
 (1.10)

The exceptions in the literature are two papers examining the effect of fatigue on the hardness of the material. The first work is Pavlou's (2002) research. Based on the tests of aluminum alloy 2024-T42, a linear dependence of the increase in HV was shown, depending on the number of cycles (n) for the given cycle amplitude. It has been shown that the degree of damage is a function of HV, depending on the number of cycles, i.e., stress:

$$D(n,\sigma) = HV(n,\sigma). \tag{1.11}$$

The second paper examining the effect of fatigue on the hardness of the material was written by Rogachev et al. (2023) on the effect of the Cu–Zn alloy material. In this case, a sheet of this bronze with a thickness of 3 mm has undergone technological alternating bending. As a result of such a process, deformations in the elastic-plastic range changed in the processed element. The starting material had a microhardness of 99 HV. After the technology used, the average cross-sectional hardness increased to 124 HV. The greatest strengthening, to the level of 130 HV, was observed on the outer surfaces, where the greatest deformations occurred, and the smallest in the central part. There, the hardness increased to 118 HV.

No more papers analyzing the effect of fatigue on hardness have been found. It seems that the task opposite to what was presented in the review of the literature on the problem under consideration may also be interesting from the cognitive point of view. During the fatigue process, the material undergoes deformation, and significant plastic deformations occur locally. These deformations can determine the microhardness variables. This process, in the case of tension-compression, may be less interesting due to the homogeneous nature of both strain and stress. However, in the case of stress and strain gradients, this process can be particularly noticeable. It appears that the simplest fatigue tests, followed by microhardness analysis, can be conducted on the basis of tests under conditions of cyclic bending, cyclic torsion, and a combination of cyclic bending and torsion. At the same time, a fractographic and topographical analysis of the fractures obtained should be carried out. In this way, we will get a picture of the hardness and surface quality for different combinations. It seems that such an image may define a previous load. Therefore, the resulting image in the combination of topography and hardness determines the previous fatigue load.

The aim of this work is to analyze the effect of fatigue on samples made of RG7 bronze on the microhardness on the fracture plane with cracks. The analysis was performed on the basis of cyclic bending, cyclic torsion, and two combinations of proportional bending and torsion at zero mean stress.

#### 2. Experimental research

Experimental studies concern the RG7 copper alloy (other designations are, for example, CuSn7Zn4Pb7, CC993K), where the elastic modulus  $E=92.14\,\mathrm{GPa}$ . This material is characterized by very high ductility (Hong, 2018; Lim *et al.*, 2009; You & Miskiewicz, 2008; Małecka *et al.*, 2023), like most materials where the main component is copper. The static properties of the tested and analyzed bronze are characterized by the yield point  $\sigma_y=120\,\mathrm{MPa}$ , ultimate stress  $\sigma_u=270\,\mathrm{MPa}$  (Małecka & Łagoda, 2024).

Fatigue tests will be performed on samples without a geometric notch of the "diabolo" type (Fig. 1) for pure symmetrical plane bending, pure double-sided torsion, and two combinations

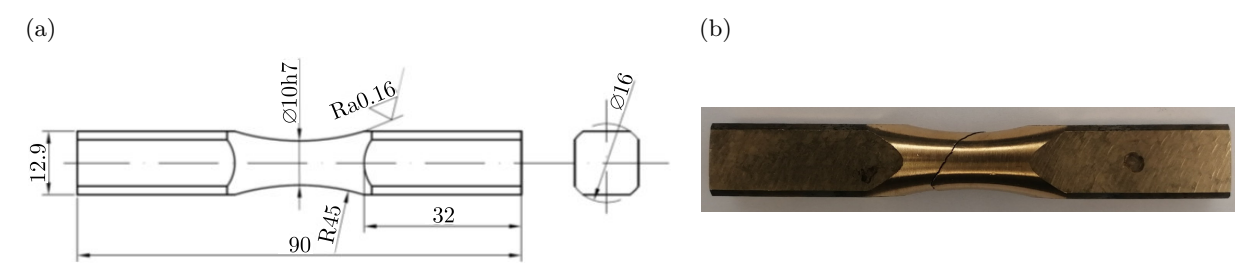


Fig. 1. "Diabolo" type specimen's dimensions: (a) working drawing; (b) photo of the sample after fatigue tests.

of proportional bending with torsion in relation to the amplitudes of stresses from torsion and bending, 0.5 and 1. This means:

$$\tau_a = 0.5\sigma_a, \qquad \tau_a = \sigma_a. \tag{2.1}$$

For the fatigue tests, a stand designed and made at the Opole University of Technology was used. Details of the operation of this stand can be found, among others, in (Małecka & Łagoda, 2024). The main principle of operation of this station is to spin the unbalanced mass, which in turn gives strength. This force, on the other hand, acts on the arm and results in a cyclically varying torque. This moment can, in effect, be split into any combination of alternating bending and torsional moments. Assuming elasticity, it can be stated that the tests are carried out under stress control. This allows the testing of materials for any combination of proportional cyclic bending and torsion.

Fatigue tests will be carried out so that the minimum fatigue life is at a high load level, giving a maximum of approx. 50000 cycles and a minimum load of at least 1000000 cycles (close to the fatigue limit). On this basis, Basquin fatigue characteristics (based on 18–20 specimens for every characteristic) written in double-logarithmic scale will be determined for each material in the form of

$$\log N_f = A_\sigma - m_\sigma \log \sigma_a \tag{2.2}$$

or

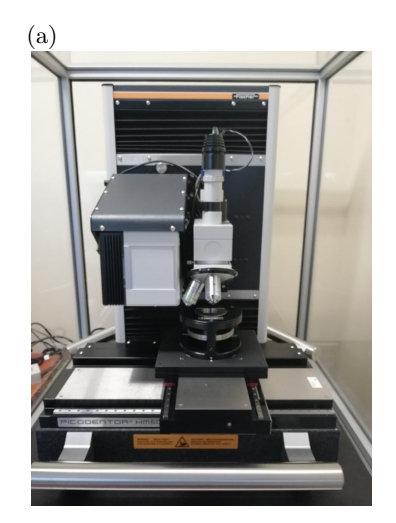
$$\log N_f = A_\tau - m_\tau \log \tau_a. \tag{2.3}$$

In the case of cyclic bending and two combinations of cyclic bending and torsion, according to Eqs. (2.1), the coefficients appearing in Eq. (2.2) are as follows:  $A_{\sigma}=26.26, m_{\sigma}=9.09$  for cyclic bending;  $A_{\sigma}=24.47, m_{\sigma}=8.85,$  and  $A_{\sigma}=25.24, m_{\sigma}=10.64$  for a combination of cyclic bending and torsion.

In the case of torsion, the coefficients in Eq. (2.3) are:  $A_{\tau} = 38.34$  and  $m_{\tau} = 15.38$ .

The nanohardness tester (Fig. 2a) (Derda et al., 2022), and the distribution of microhardness in the cross-section of the damaged material will be presented. Additionally, an optical microscope was used (Fig. 2b). Static and uniaxial tensile-compression tests were performed on a standard INSTRON fatigue stand.

An important characteristic of construction materials is their hardness, which depends on properties such as ductility, stiffness, plasticity, deformability, and strength of the tested material. As part of the research, hardness distribution contour lines will be determined on the cross-sections of samples, both in the initial state and after being subjected to fatigue tests. The assessment of changes in the properties of the tested materials will be carried out based on Martens hardness measurements, which are a hardness testing method based on continuous measurement of force as a function of displacement. Unlike standard methods, which include



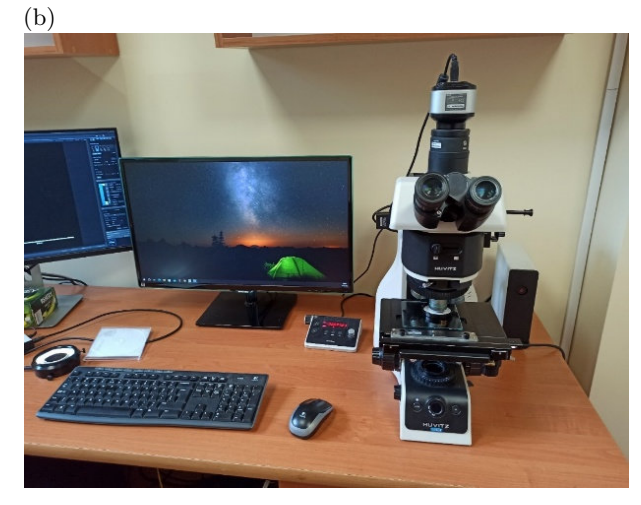


Fig. 2. Research devices: (a) nanohardness stand PICODENTOR HM 500 produced by Helmut Fischer; (b) optical microscope.

the Brinell, Rockwell, and Vickers methods, it is not based on a hardness reading from the measurement of the surface area of the indentation formed under the influence of a given force, but on a computer analysis of the obtained penetration curve. The measurement result is presented in the form of a loading and unloading curve as a function of the force applied to the indenter from the depth of penetration. Based on the obtained results, it will be possible to determine the stiffness of the sample read from the loading curve, the instrumental modulus of elasticity (approximately equal to the modulus of elasticity of the material), instrumental hardness, work of deformation (energy of elastic and plastic deformation of the material), etc. The tests will be performed using a system for measurement of nano- and microhardness according to the Martens method, in accordance with the PN EN ISO 14577 standard, PICODENTOR HM 500 (Fig. 2a) equipped with WIN-HCU software, which allows the use of forces applied to the indenter in the range of 0.005 mN-500 mN.

### 3. Microhardness measurements

Hardness measurements were made on selected (best suited to the fatigue characteristics) samples according to Table 1. For various bending-torsion combinations, samples (23, 44, 58, 21) were selected for a durability of approximately 500000 cycles. In addition, the sample was analyzed and not subjected to any load in the conditions of uniaxial static stretching and cyclic stretching-compression.

Table 1. Summary	of sample	numbers,	number	of cycles	to failure	and load	method.

Sample	Number	$N_f$ (cycles)	
Withouth loading	00	_	
Static tension	02	0.5	
Tension-compression	06	5924	
$\tau_a = 0$	23	571257	
$\sigma_a = 0.5\tau_a$	44	776838	
$\sigma_a = \tau_a$	58	522700	
$\sigma_a = 0$	21	481710	

Metallographic sections for macroscopic examinations and microhardness measurements were made from samples after fatigue tests, and the test surface was a cross-section perpendicular to

the axis of the sample at a distance of up to 3 mm from the obtained fracture. The samples were cut on a disc cutter with intensive cooling, and then embedded in a plastic mass. The samples prepared in this way were ground manually on abrasive papers of decreasing gradation (#350, #600, #800, #1200, #2000) and then mechanically polished on synthetic cloths using a water suspension of aluminum oxide ( $Al_2O_3$ ). Finally, the samples were polished on a vibratory polisher and chemically etched with a reagent for etching copper and its alloys ( $HCl+FeCl_3+H_2O$ ) to eliminate the effect of surface strengthening after metallographic preparation. The prepared microsection is shown in Fig. 3a and Fig. 4a.

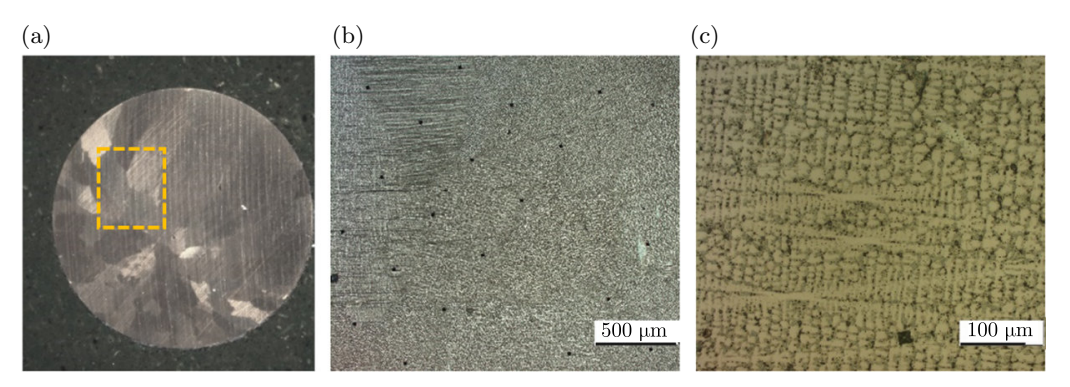


Fig. 3. Bronze sample in the initial state: (a) macro image with the micro observation point marked; (b), (c) bronze microstructure over  $50 \times$  and  $200 \times$ .

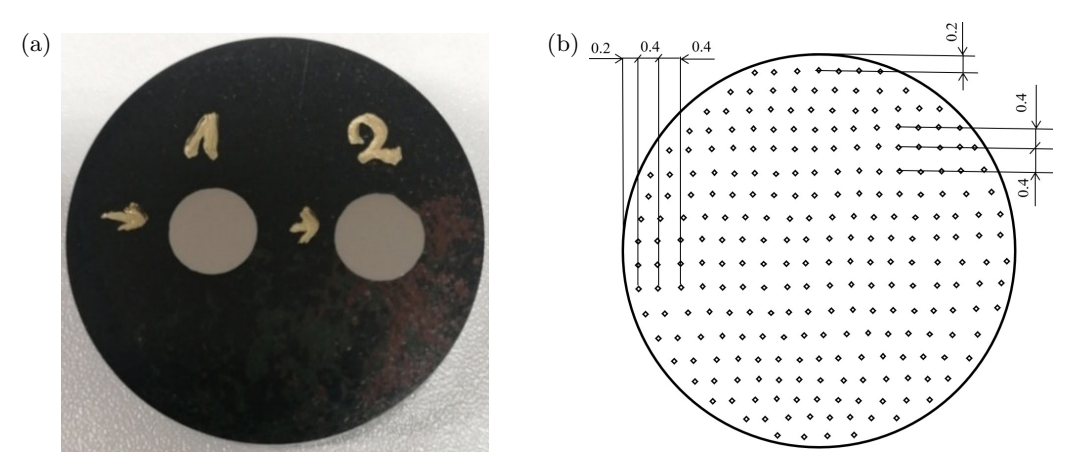


Fig. 4. Sample for microhardness testing: (a) macro-photo of the micro-section before microhardness measurement; (b) measurement scheme (500 to 600 points depending on the sample).

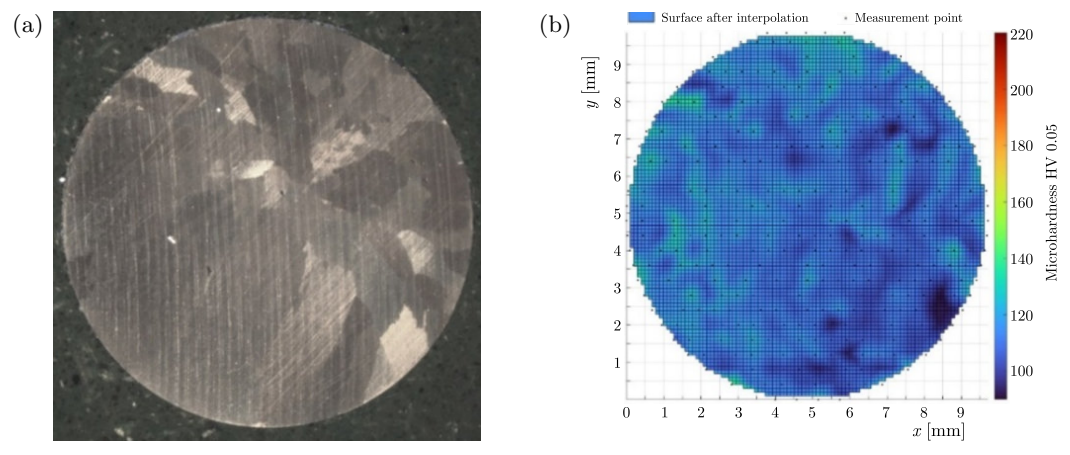


Fig. 5. Sample before loading (00): (a) macroscopic photo of the micro-section surface before microhardness measurement; (b) microhardness contour lines on the surface of the micro-section.

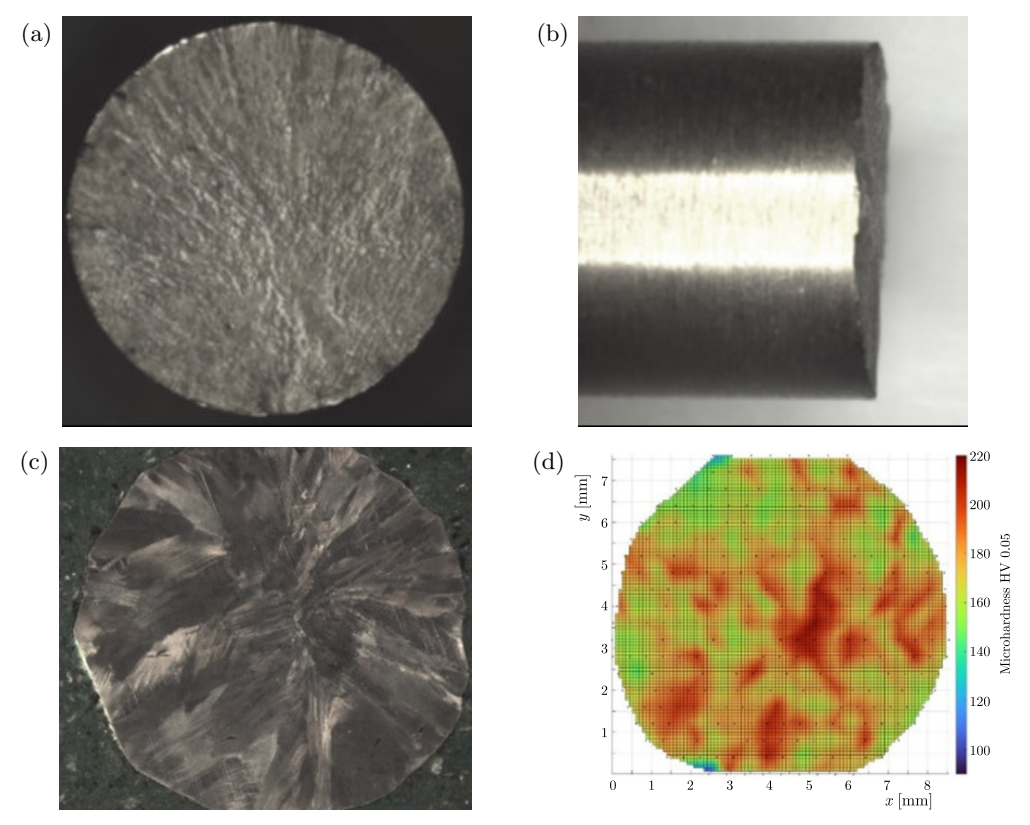


Fig. 6. Sample (02) after the static tensile test: (a) macroscopic photo of the scrap surface; (b) macroscopic photo of the crack direction; (c) macroscopic photo of the micro-section surface before microhardness measurement; (d) microhardness contour lines on the surface.

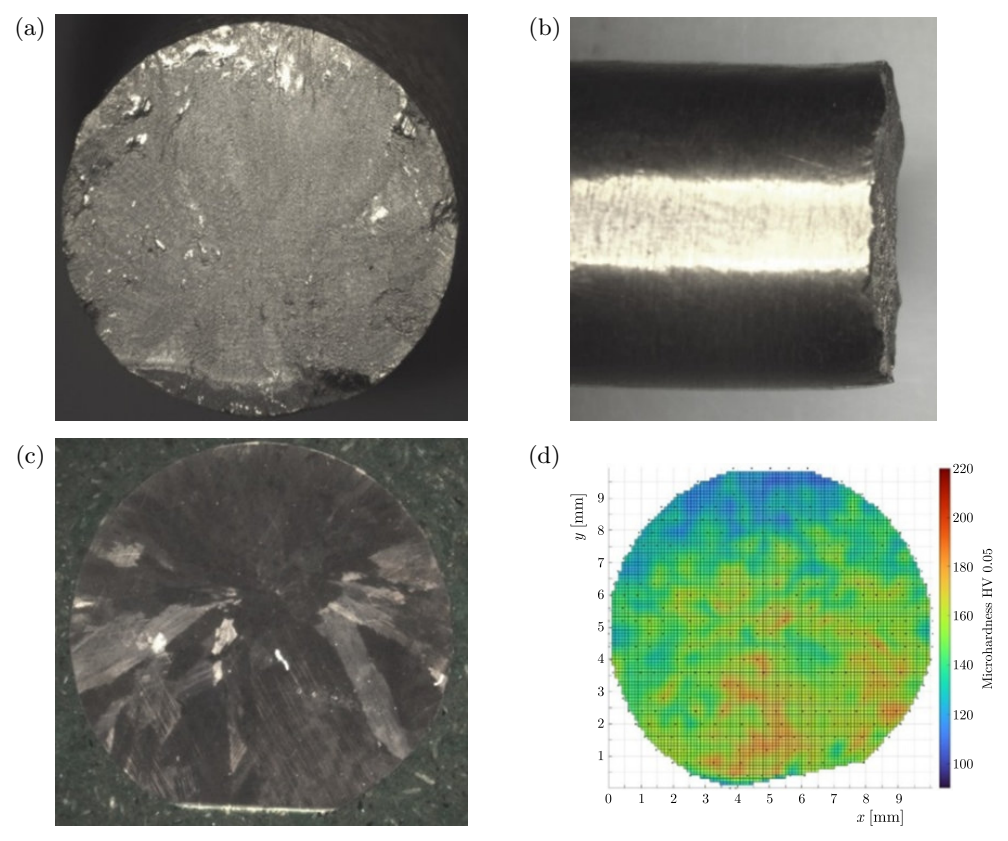


Fig. 7. Sample (06) after the tensile-compression test: (a) macroscopic photo of the scrap surface; (b) macroscopic photo of the crack direction; (c) macroscopic photo of the micro-section surface before microhardness measurement; (d) microhardness contour lines on the surface.

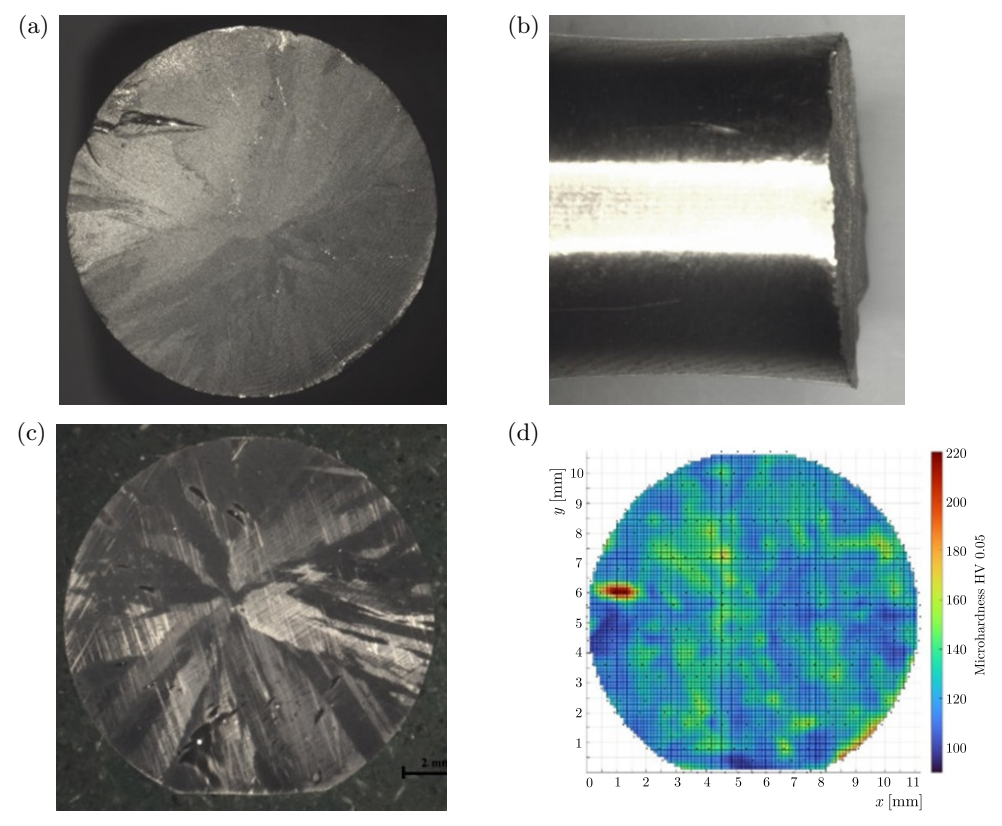


Fig. 8. Sample (23) after the cyclic bending test: (a) macroscopic photo of the scrap surface; (b) macroscopic photo of the crack direction; (c) macroscopic photo of the micro-section surface before microhardness measurement; (d) microhardness contour lines on the surface.

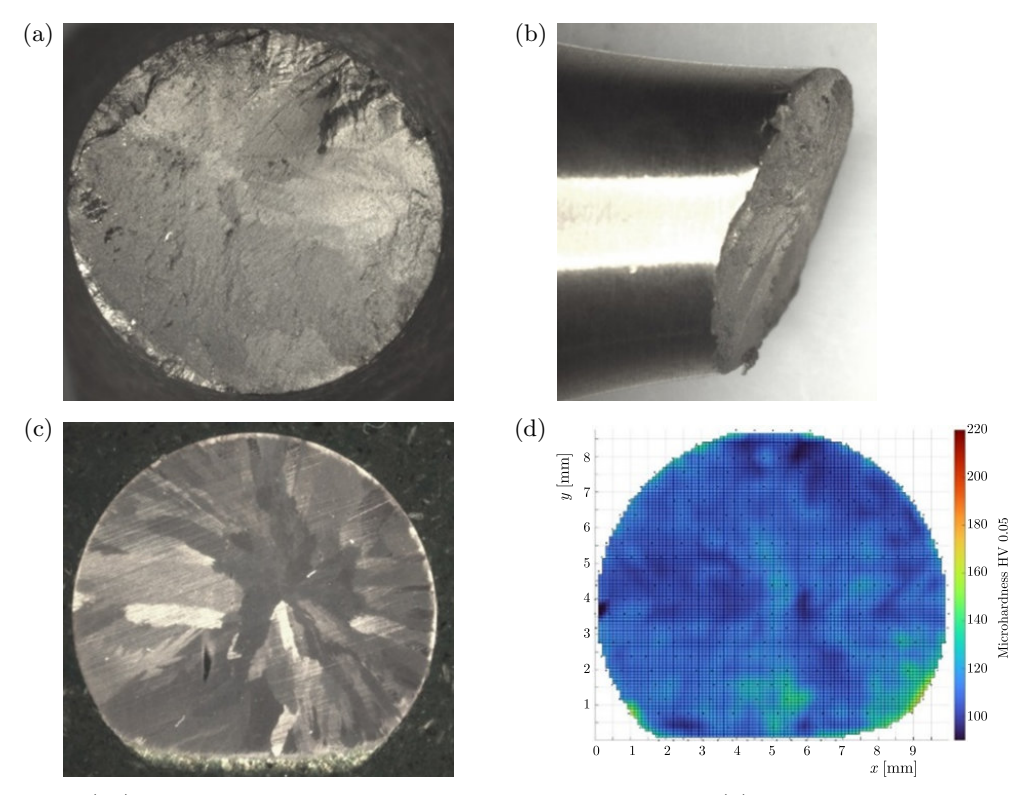


Fig. 9. Sample (44) after cyclic bending with torsion test  $\sigma_a = 0.5\tau_a$ : (a) macroscopic photo of the scrap surface; (b) macroscopic photo of the scrap surface before microhardness measurement; (c) microhardness contour lines on the surface.

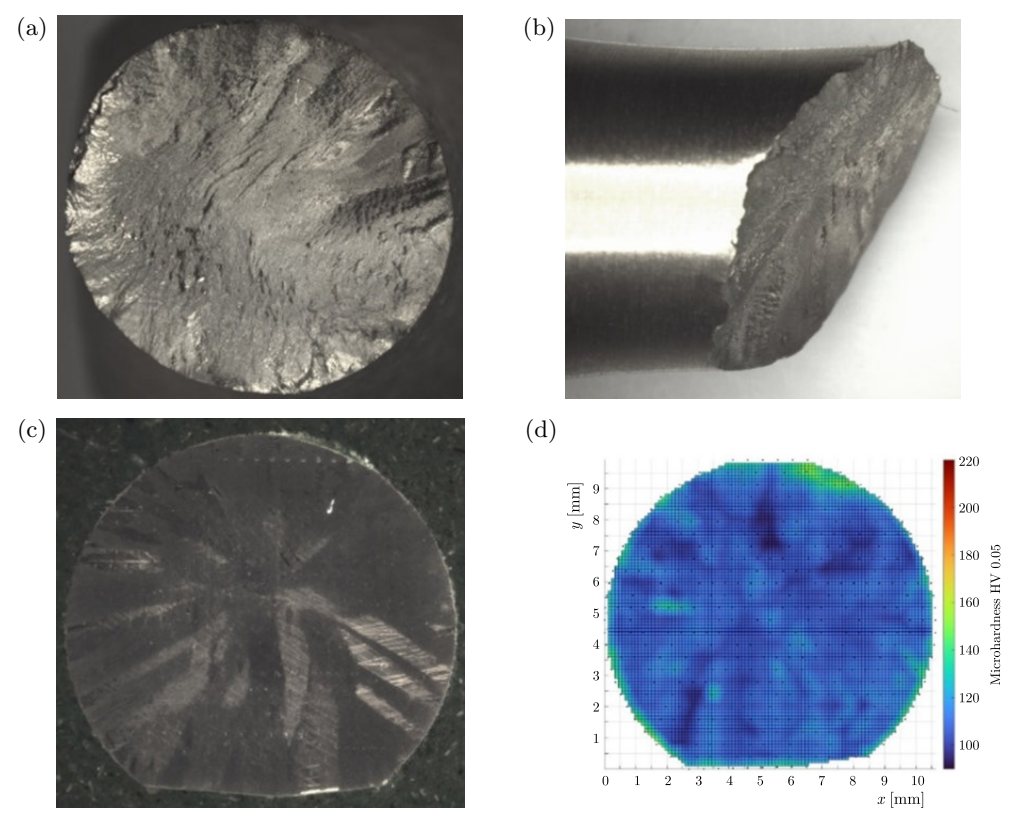


Fig. 10. Sample (58) after the cyclic bending test with torsion  $\sigma_a = \tau_a$ : (a) macroscopic photo of the scrap surface; (b) macroscopic photo of the crack direction; (c) macroscopic photo of the micro-section surface before microhardness measurement; (d) microhardness contour lines on the surface.

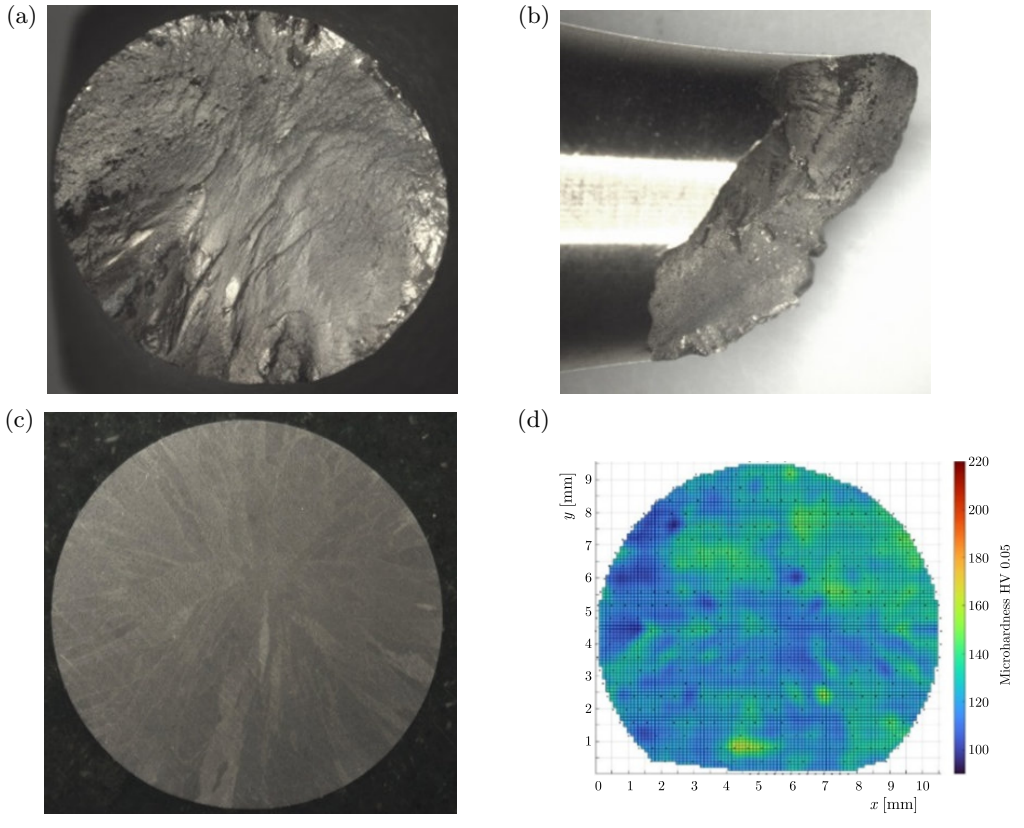


Fig. 11. Sample (21) after the cyclic torsion test: (a) macroscopic photo of the scrap surface; (b) macroscopic photo of the crack direction; (c) macroscopic photo of the micro-section surface before microhardness measurement; (d) microhardness contour lines on the surface.

The structure of the analyzed samples is typical for tin-lead bronzes, in which the  $\alpha$  solid solution with the eutectoid phase  $(\alpha + \delta)$  occurring in the interdendritic spaces and lead precipitates can be identified (Figs. 3b and 3c). Microhardness measurements were carried out using the Martens method, for which a Vickers indenter was used, which was loaded with a force of  $500\,\mathrm{mN}$  (50 g) for 20 seconds. Measurement points were made as described in Fig. 4b.

Figure 5b and part (d) of Figs. 6–11 show the contour lines of the microhardness distribution for individual samples, i.e., the initial state (00), after the static tensile test (02), after the tensile-compression fatigue test (06), after cyclic bending (23), cyclic torsion (21), a combination of bending and torsion with a proportionality factor of 0.5 (44) and a proportionality factor of 1 (58) in combination with the image of the obtained fractures (part (a) of Figs. 5–11) along with the direction of the crack (part (b) of Figs. 6–11) and macrostructure (Fig. 5a and part (c) of Figs. 6–11). Pictures were taken with an optical microscope at a magnification of about 20×. In the case of cyclic bending (Fig. 8), a significant local increase in hardness can be observed, which is probably due to static fracture at this location.

Figure 12 shows the minimum, average, and maximum values of microhardness obtained for individual samples.

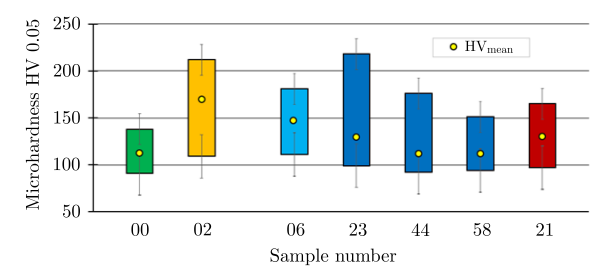


Fig. 12. List of microhardness for individual tested samples.

## 4. Analysis of the obtained measurement results

Table 2 presents the average microhardness values of the tested samples, taking into account the minimum and maximum values in the analyzed areas, shown in Fig. 5b and part (d) of Figs. 6–11. In addition, the maximum increase in microhardness in relation to the maximum microhardness of the unloaded sample was summarized. The maximum increase was obtained for the static tensile and cyclic bending tests. Then the deformations were the greatest, and locally the most significant hardness increase occurred. A relatively large increase in microhardness also occurred in the case of stretching and the combination of cyclic bending and torsion with small shear stresses. The smallest increase in maximum microhardness occurred in the case of a combination of bending and torsion with significant shear stresses.

Sample		$\mathrm{HV}_{\mathrm{min}}$	$\mathrm{HV}_{\mathrm{max}}$	$\mathrm{HV}_{\mathrm{mean}}$	Max increase HV <sub>max</sub> [%]
00	Without loading	91	138	114	_
02	Static tension	109	212	174	54
06	Tension-compression	111	181	148	31
23	Bending $\tau_a = 0$	99	218	126	57
44	$\sigma_a = 0.5 \cdot \tau_a$	92	176	113	28
58	$\sigma_a = \tau_a$	94	151	113	9
21	Torsion $\sigma_a = 0$	97	165	124	20

Table 2. List of minimum, maximum, and medium microhardnesses HV.

In the case of sample 00 (no load condition – starting material), the hardness of the sample oscillated in the range of 91 HV–138 HV and was clearly related to the heterogeneity of the

material structure, which can be seen in Fig. 5b. The largest increase in the average hardness in relation to the initial sample (00) (114 HV), which is 53 % (174 HV), was recorded for the sample after the static tensile test (02). Additionally, for this sample, the maximum hardness of 212 HV was obtained, i.e., an 85 % increase compared to the average hardness of the sample in the initial state, and it was located mainly in the central part of the cross-section. In the case of the sample that was subjected to the cyclic tensile test with compression (06) and subjected to bending (23), a systematic decrease in average hardness was observed, to the respective values of 148 HV and 126 HV, but these values are higher than the hardness of the initial sample by 30 % and 10 %, respectively. In all cases, the fracture formed was perpendicular to the axis of the sample (part (b) of Figs. 6–8), and the maximum hardness was identified in the areas where cracks were initiated (part (a) of Figs. 6–8).

The samples after the bending and torsion tests carried out at different loads (44 and 58) were characterized by an average hardness at the same level as in the case of the sample in the initial state (00) and both amounted to 113 HV. However, the maximum hardness in the analyzed areas was 176 HV and 151 HV, respectively, and it was identified near the edge of the sample (Fig. 9d and Fig. 10d). In the last case, i.e., the bending sample (21), there was a slight, 9% increase in the average cross-sectional hardness (124 HV); however, the maximum hardness, at the level of 165 HV, was identified in different cross-sectional areas (Fig. 11d). A different nature of the resulting breakthroughs was also observed. In the case of samples subjected to bending with torsion, the fracture was formed at an angle of approx.  $70^{\circ}-75^{\circ}$  to the axis of the sample, while in the case of torsion, this angle is approx.  $50^{\circ}$ .

#### 5. Conclusions

The measurement and analysis of the microhardness of the RG7 bronze fracture plane showed that:

- every static or fatigue damage causes an increase in microhardness in relation to the unloaded material;
- the greatest increase in microhardness occurs at the point of the greatest unloading in the presence of a stress gradient;
- the highest increase in maximum microhardness was obtained for the static tensile test and for cyclic bending (in these cases, we are dealing with the largest surface on which destruction occurs at the initiation stage);
- the smallest increase in maximum microhardness was obtained for the combination of cyclic bending and torsion with a significant shear stress coming from torsion.

#### Acknowledgments

This work was financially supported by the Opole University of Technology as part of the GRAS project no. 260/23.

#### References

- Assi, A.D., & Alkalali, R.H.M. (2021). Fatigue limit prediction based on hardness for both steel and aluminum alloys. IOP Conference Series: Materials Science and Engineering, 1105, Article 012044. https://doi.org/10.1088/1757-899X/1105/1/012044
- 2. Bandara, C.S., Siriwardane, S.C., Dissanayake, U.I., & Dissanayake, R. (2015). Developing a full range S-N curve and estimating cumulative fatigue damage of steel elements. *Computational Materials Science*, 96(Part A), 96–101. https://doi.org/10.1016/j.commatsci.2014.09.009

3. Bandara, C.S., Siriwardane, S.C., Dissanayake, U.I., & Dissanayake, R. (2016). Full range S–N curves for fatigue life evaluation of steels using hardness measurements. *International Journal of Fatigue*, 82(Part 2), 325–331. https://doi.org/10.1016/j.ijfatigue.2015.03.021

- Derda, S., Karolczuk, A., Prażmowski, M., Kurek, A., Wachowski, M., & Paul, H. (2022). Fatigue life and cyclic creep of tantalum/copper/steel layerwise plates under tension loading at room temperature. *International Journal of Fatigue*, 162, Article 106977. https://doi.org/10.1016/j.ijfatigue. 2022.106977
- 5. Görzen, D., Ostermayer, P., Lehner, P., Blinn, B., Eifler, D., & Beck, T. (2022). A new approach to estimate the fatigue limit of steels based on conventional and cyclic indentation testing. *Metals*, 12(7), Article 1066. https://doi.org/10.3390/met12071066
- 6. Hong, S.I. (2018). Criteria for predicting twin-induced plasticity in solid solution copper alloys. *Materials Science and Engineering: A*, 711, 492–497. https://doi.org/10.1016/j.msea.2017.11.076
- 7. James, M.N., Ting, S.-P., Bosi, M., Lombard, H., & Hattingh, D.G. (2009). Residual strain and hardness as predictors of the fatigue ranking of steel welds. *International Journal of Fatigue*, 31(8–9), 1366–1377. https://doi.org/10.1016/j.ijfatigue.2009.03.006
- 8. Kloos, K.H., & Velten, E. (1984). Calculation of the fatigue strength of plasma nitrided component-like samples taking into account the hardness and residual stress profile (in German). *Konstruktion*, 36(5), 181–8.
- 9. Kondo, Y., Sakae, C., Kubota, M., & Kudou, T. (2003). The effect of material hardness and mean stress on the fatigue limit of steels containing small defects. Fatigue & Fracture of Engineering Materials & Structures, 26(8), 675–682. https://doi.org/10.1046/j.1460-2695.2003.00656.x
- 10. Kurek, A., Kurek, M., & Łagoda, T. (2019). Stress-life curve for high and low cycle fatigue. *Journal of Theoretical and Applied Mechanics*, 57(3), 677–684. http://doi.org/10.15632/jtam-pl/110126
- 11. Li, Z., Wang, Q., Luo, A.A., Fu, P., & Peng, L. (2015). Fatigue strength dependence on the ultimate tensile strength and hardness in magnesium alloys. *International Journal of Fatigue*, 80, 468–476. https://doi.org/10.1016/j.ijfatigue.2015.07.001
- 12. Lim, C.-B., Kim, K.S., & Seong, J.B. (2009). Ratcheting and fatigue behavior of a copper alloy under uniaxial cyclic loading with mean stress. *International Journal of Fatigue*, 31(3), 501–507. https://doi.org/10.1016/j.ijfatigue.2008.04.008
- 13. Małecka, J., & Łagoda, T. (2024). Use of the biaxial coefficient in determining life for a combination of cyclic bending and torsion of bronze RG7. *Journal of Theoretical and Applied Mechanics*, 62(3), 547–560. https://doi.org/10.15632/jtam-pl/188855
- 14. Małecka, J., Łagoda, T., Głowacka, K., & Vantadori, S. (2023). Influence of plastic deformations on both yield strength and torsional fatigue life of non-ferrous alloys. Fatigue & Fracture of Engineering Materials & Structures, 46(6), 2080–2095. https://doi.org/10.1111/ffe.13982
- 15. Mitchell, M.R. (1996). Fundamentals of modern fatigue analysis for design. In ASM Handbook Committee (Eds.), ASM Handbook: Vol. 19. Fatigue and Fracture (pp. 227–249). ASM International. https://doi.org/10.31399/asm.hb.v19.a0002364
- 16. Pang, J.C., Li, S.X., Wang, Z.G., & Zhang, Z.F. (2014). Relations between fatigue strength and other mechanical properties of metallic materials. Fatigue & Fracture of Engineering Materials & Structures, 37(9), 958–976. https://doi.org/10.1111/ffe.12158
- 17. Pang, J.C., Li, S.X., & Zhang, Z.F. (2013). High-cycle fatigue and fracture behaviours of Cu-Be alloy with a wide strength range. Fatigue & Fracture of Engineering Materials & Structures, 36(2), 168–176. https://doi.org/10.1111/j.1460-2695.2012.01710.x
- 18. Pavlou, D.G. (2002). A phenomenological fatigue damage accumulation rule based on hardness increasing, for the 2024-T42 aluminum. *Engineering Structures*, 24(11), 1363–1368. https://doi.org/10.1016/S0141-0296(02)00055-X
- 19. Roessle, M.L., & Fatemi, A. (2000). Strain-controlled fatigue properties of steels and some simple approximations. *International Journal of Fatigue*, 22(6), 495–511. https://doi.org/10.1016/S0142-1123(00)00026-8

- Rogachev, S.O., Shelest, A.E., Perkas, M.M., Andreev, V.A., Tabachkova, N.Yu., Yusupov, V.S., Ten, D.V., Isaenkova, M.G., & Krymskaya, O.A. (2023). Effect of alternating bending on structure, texture, and mechanical properties of Cu–Zn alloy. *Journal of Materials Engineering and Perfor*mance, 33(3), 1241–1249. https://doi.org/10.1007/s11665-023-08050-w
- 21. Shamsaei, N., & Fatemi, A. (2009). Effect of hardness on multiaxial fatigue behaviour and some simple approximations for steels. Fatigue & Fracture of Engineering Materials & Structures, 32(8), 631–646. https://doi.org/10.1111/j.1460-2695.2009.01369.x
- 22. Shiozawa, K., Sakai, T. et al. (1996). Databook on fatigue strength of metallic materials (Vols. 1–3). Elsevier & JSMS.
- 23. Sriraman, K.R., Raman, S.G.S., & Seshadri, S.K. (2007). Influence of crystallite size on the hardness and fatigue life of steel samples coated with electrodeposited nanocrystalline Ni–W alloys. *Materials Letters*, 61(3), 715–718. http://doi.org/10.1016/j.matlet.2006.05.049
- 24. Xin, H., Correia, J.A.F.O., Veljkovic, M., Berto, F., & Manuel, L. (2021). Residual stress effects on fatigue life prediction using hardness measurements for butt-welded joints made of high strength steels. *International Journal of Fatigue*, 147, Article 106175. https://doi.org/10.1016/j.ijfatigue.2021.106175
- 25. You, J.-H., & Miskiewicz, M. (2008). Material parameters of copper and CuCrZr alloy for cyclic plasticity at elevated temperatures. *Journal of Nuclear Materials*, 373(1–3), 269–274. https://doi.org/10.1016/j.jnucmat.2007.06.005

Manuscript received May 19, 2025; accepted for publication August 20, 2025; published online October 30, 2025.